Advanced Monte Carlo modeling of prompt fission neutrons for thermal and fast neutron-induced fission reactions on ^{239}Pu

P. Talou,[1,*] B. Becker,[2] T. Kawano,[1] M. B. Chadwick,[3] and Y. Danon[2]
[1]*T-2 Nuclear Theory Group, Los Alamos National Laboratory, Los Alamos, New Mexico 87545, USA*
[2]*Gaerttner LINAC Laboratory, Rensselaer Polytechnic Institute, New York 12180, USA*
[3]*X-CP, Los Alamos National Laboratory, Los Alamos, New Mexico 87545, USA*
(Received 4 April 2011; published 23 June 2011)

Prompt fission neutrons following the thermal and 0.5 MeV neutron-induced fission reaction of ^{239}Pu are calculated using a Monte Carlo approach to the evaporation of the excited fission fragments. Exclusive data such as the multiplicity distribution $P(\nu)$, the average multiplicity as a function of fragment mass $\overline{\nu}(A)$, and many others are inferred in addition to the most used average prompt fission neutron spectrum $\chi(E_{\rm in}, E_{\rm out})$, as well as average neutron multiplicity $\overline{\nu}$. Experimental information on these more exclusive data help constrain the Monte Carlo model parameters. The calculated average total neutron multiplicity is $\overline{\nu}_c = 2.871$ in very close agreement with the evaluated value $\overline{\nu}_e = 2.8725$ present in the ENDF/B-VII.0 library. The neutron multiplicity distribution $P(\nu)$ is in very good agreement with the evaluation by Holden and Zucker. The calculated average spectrum differs in shape from the ENDF/B-VII.0 spectrum, evaluated with the Madland-Nix model. In particular, we predict more neutrons in the low-energy tail of the spectrum (below about 300 keV) than the Madland-Nix calculations, casting some doubts on how much scission neutrons contribute to the shape of the low-energy tail of the spectrum. The spectrum high-energy tail is very sensitive to the total kinetic energy distribution of the fragments as well as to the total excitation energy sharing at scission. Present experimental uncertainties on measured spectra above 6 MeV are too large to distinguish between various theoretical hypotheses. Finally, comparisons of the Monte Carlo results with experimental data on $\overline{\nu}(A)$ indicate that more neutrons are emitted from the light fragments than the heavy ones, in agreement with previous works.

DOI: 10.1103/PhysRevC.83.064612 PACS number(s): 25.85.Ec, 24.10.Pa

I. INTRODUCTION

Primary excited fission fragments release energy and angular momentum by emitting neutrons and γ rays, until they reach a more stable configuration, often their ground state. Those particles, called *prompt* neutrons and γ rays, shed some light on the fission process near scission, and represent an important link in our understanding of the pre- and postscission physics. In particular, they can inform us on the particular fragment shape configurations that are produced near the scission point, and how much excitation energy and angular momentum are present in the fragments right after scission.

From a more applied perspective, prompt fission neutrons play a very important role in neutronics calculations for nuclear applications. The recent surge of interest in innovative nuclear fuel cycles and the accompanying new requirements for stringent safety and security margins for the next generation of nuclear reactors also pushes for better accuracies in evaluated nuclear data. Recently it was shown that estimated uncertainties in the prompt fission neutron spectrum from low-energy neutron-induced reactions can significantly impact the results of transport simulations for critical assemblies [1] as well as reactor sensitivity calculations. In fact, even for the most well-known actinides, significant uncertainties remain in the low-energy part of the spectrum, below ~500 keV, as well as in the high-energy tail, above ~6 MeV. At low outgoing neutron energies, measurements are made very difficult owing to the multiple scattering from ambient neutrons and from energy cuts in the detection efficiency of most current neutron detectors. At the opposite side of the spectrum, the measurement statistics become very poor for neutrons above about 6 MeV.

The low-energy part of the spectrum has been the subject of great interest over the years as some authors have postulated the existence of scission neutrons which would contribute to an increase of neutron production below 0.5 MeV [2]. In this article, scission neutrons refer to all neutrons emitted before the fission fragments are fully accelerated, that is, neutrons emitted during the descent from the saddle to the scission point, or right at the time of the neck rupture.

Over the last 30 years, the Los Alamos or Madland-Nix (MN) model [3] has played a key role in providing a powerful yet simple tool to calculate the average prompt fission neutron spectrum (PFNS) and multiplicity (PFNM) for many actinides and over many incident neutron energies, with only a handful of free model parameters. The MN model has been very successful in reproducing and predicting PFNS for a large set of actinides. However, its predictions remain limited to those two average quantities. While it provides a very important and convenient tool for evaluating nuclear data, and has been extended somewhat to predict additional quantities [4–6], this model can hardly be extended any further to provide more insights in the physics near the scission point.

To better analyze and predict postscission data, one has to gain access to more exclusive data such as the neutron

*talou@lanl.gov

 ©2011 American Physical Society

multiplicity distribution $P(\nu)$ or the average PFNM as a function of the fission fragment mass $\overline{\nu}(A)$. Some time ago we developed a Monte Carlo approach to study the detailed evaporation mechanism from the excited primary fission fragments [7,8], inspired by the pioneer work of Browne and Dietrich [9]. Within this model, neutrons are emitted sequentially from a temperature-dependent Weisskopf spectrum, assuming that γ rays are only emitted following the neutron emissions, until the excitation energy falls below the neutron separation energy of the last decaying fragment. Prompt fission neutrons can then be studied on an event-by-event basis, and new details about the evaporation mechanism can be studied. A similar approach was adopted recently by Randrup and Vogt [10,11], as well as by Litaize and Serot [12].

In the present paper, we focus on the low-energy (thermal and 0.5 MeV) neutron-induced fission of ^{239}Pu for which relatively good experimental data exist on PFNS and PFNM, as well as more exclusive data such as $\overline{\nu}(A)$.

In Sec. II we recall the main elements of our Monte Carlo approach for which a slightly different version was already presented partially in Ref. [7]. An important ingredient in this approach is the initial distribution of the preneutron emission fission fragment yields as a function of mass, charge, and total kinetic energy $Y(A, Z, TKE)$, and is discussed at some length in Sec. III. We then address the important question of how the total excitation energy available in the fissioning system is shared between the two nascent fragments. Section V presents and discusses numerical results in view of existing experimental data sets and other model calculations. The conclusion summarizes this work, and emphasizes the importance of specific new experiments addressing some of the key uncertainties of the current method.

II. MONTE CARLO APPROACH TO FISSION FRAGMENT EVAPORATION

This approach has been described at some length in previous publications [7,13]. However, it remains central to most of the ensuing discussion and its important details and assumptions are worth recalling here.

In this work we make the assumption that neutrons are emitted only from fully accelerated fragments, and that no emission occurs during the descent from saddle to scission, or even at the time of the neck rupture.

The starting point is the distribution of primary fission fragments, after scission but prior to prompt neutron emissions. In low-energy neutron induced fission of ^{239}Pu, the fragment mass distribution is strongly asymmetric as influenced by the presence of the $A = 132$ shell closure, with a very small component in the symmetric region near $A = 120$. The charge distribution of the fragments is not as well known, but is believed to follow the unchanged charge distribution (UCD) with a small shift of ± 0.5 away from symmetry [14]. Knowing the mass A and charge Z of the fragments is not enough though, as the initial excitation energy in the fragments is needed to start the sequential emission of neutrons. The total kinetic energy (TKE) of the recoiling fragments has been measured by several groups, and is usually known as a function of the fragment mass. From this quantity, and for a given pair of fission fragments, the total excitation energy TXE to be shared among the light and heavy fragments is simply given by

$$\begin{aligned} TXE &= Q_f + E_n^{\text{inc}} + B_n(A_c, Z_c) - TKE \\ &= M_n(A_l, Z_l) + M_n(A_h, Z_h) - M_n(A_c, Z_c) \\ &\quad + E_n^{\text{inc}} + B_n(A_c, Z_c) - TKE, \end{aligned} \tag{1}$$

where Q_f is the Q-value of the fission reaction, M_n represent the nuclear masses for the light (A_l, Z_l) and heavy (A_h, Z_h) fragments, and for the fissioning compound nucleus (A_c, Z_c); E_n^{inc} is the kinetic energy of the incident neutron, and $B_n(A_c, Z_c)$ is the neutron binding energy of the compound nucleus.

This total excitation energy will be fully dissipated through the emission of neutrons and γ rays, but the exact distribution of TXE among the two fragments remains an open question. At this stage, let us introduce the parameter R_T as

$$R_T = T_0^l / T_0^h, \tag{2}$$

where T_0^l and T_0^h represent the initial temperatures in the light and heavy fragments. In the original Los Alamos model [3], thermal equilibrium between the two nascent fragments at scission is assumed, that is, R_T equals unity. However, there is now strong evidence that this assumption fails when the excitation energy is relatively low [15,16], and that the light fragment gets a larger share of TXE. We discuss this question further in the next section.

To perform a full Hauser-Feshbach computation on the excited primary fragments, one would need to know the initial spin and parity distributions, and follow (J, π) conservation rules all the way down to the ground state or isomeric state in the final residual nucleus. Here we approximate the decay process by assuming that prompt γ rays are emitted only after all prompt neutrons are evaporated, and therefore neglect the competition between prompt neutrons and γ rays.

The continuum level density in the fragments is represented by the Gilbert-Cameron-Ignatyuk formalism [17,18]. The level density is given by a constant-temperature formula at low energies connected to a Fermi-gas formula at higher energies. In addition, the level density parameter a is a function of the excitation energy to include the damping of shell effects as the excitation energy increases.

Following Weisskopf [19], neutrons are emitted from an evaporation spectrum at temperature T,

$$\rho(\epsilon_n) = \epsilon_n \exp(-\epsilon_n / T), \tag{3}$$

where ϵ_n is the neutron kinetic energy in the center-of-mass reference frame. The $(i-1)$th residual nucleus $(A-1, Z)$ is then formed with an excitation energy

$$U_{\{i-1\}} = U_i - B_n^i - \epsilon_n. \tag{4}$$

The neutron binding energy B_n^i correspond to the ith nucleus in the decay chain. At some point the residual energy becomes small enough that no more neutrons can be emitted, and the residual excitation energy is then dissipated through prompt γ rays.

In this approach Monte Carlo samplings are performed on the fission fragment yields, as well as on the evaporation

spectra at each step of the decay. The result is a large data file containing millions of histories of successive neutron emissions, from which a lot of information can be extracted, in complete analogy with experimental output. Alternatively, the analysis can and has been performed on-the-fly to save computer memory space.

Because both neutron kinetic energy and angle of emission are recorded for each event, correlated and exclusive data can be assessed, such as the neutron multiplicity distribution $P(\nu)$, the average neutron multiplicity as a function of fragment mass and kinetic energy $\overline{\nu}(A, TKE)$, exclusive spectrum for a given neutron multiplicity $\chi(E_{\rm out})_{|\nu=n}$, and neutron-neutron energy and angular correlations. Such data are invaluable to better understand the fission process near the scission point.

III. PRIMARY FISSION FRAGMENT DISTRIBUTIONS

As pointed out in the previous section, the primary fission fragment distribution as a function of mass A, charge Z, and total kinetic energy TKE is the starting point for the Monte Carlo evaporation of the fragments. In the present work, this distribution has been reconstructed in the following way.

The fission fragment mass distribution $Y(A)$ was measured by several authors: Nishio *et al.* [20], Wagemans *et al.* [21], Surin *et al.* [22], and Akimov *et al.* [23], and is shown in Fig. 1. Tsuchiya *et al.* [24] also measured this distribution, but with a relatively poor mass resolution that cannot be used for the present purpose. While the familiar asymmetric mass yield curve is well reproduced by all experiments, nonnegligible differences appear, especially for the data of Nishio *et al.* compared to all others near the peaks of the distribution. Figure 2 shows the same data sets but in log scale to illustrate differences near symmetry and in the tail of the distribution where the yields are smallest. Again, the data set

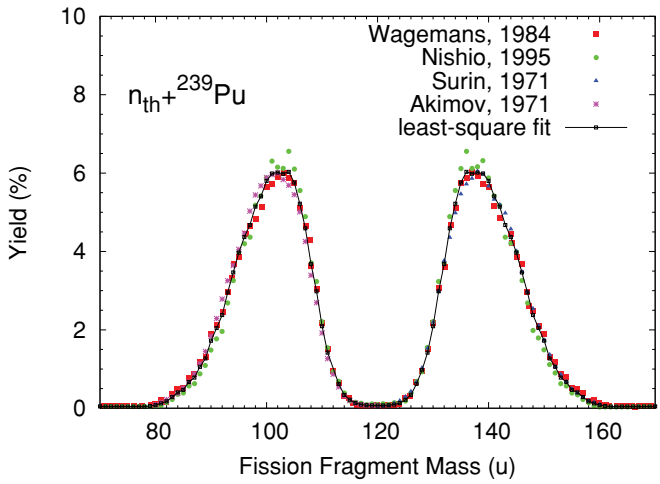

FIG. 1. (Color online) Primary fission fragment mass yields for thermal neutrons induced fission of ^{239}Pu, as measured by Nishio *et al.* [20], Wagemans *et al.* [21], Surin *et al.* [22], and Akimov *et al.* [23]. The black squares connected by lines represent the result of a least-square fit of all experimental data sets.

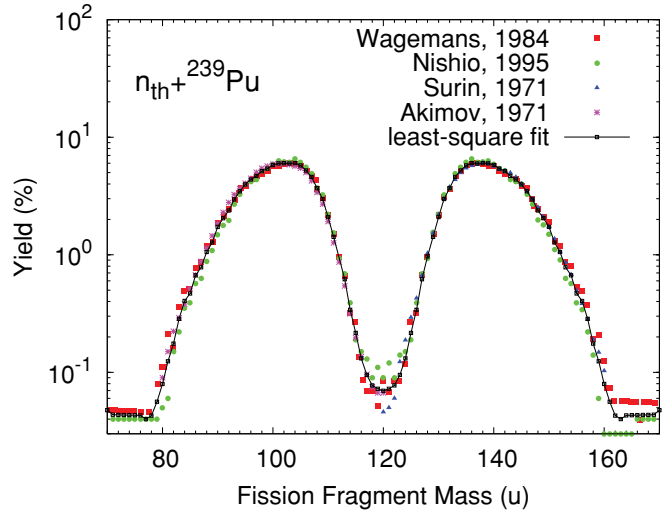

FIG. 2. (Color online) The results shown in Fig. 1 are plotted in log scale to better visualize the low yields near the symmetric region and in the tail of the distribution.

of Nishio *et al.* departs somewhat from other experimental results.

We have performed a least-square fit of the experimental mass yields to obtain our "best" estimate of $Y(A)$. We also constrained the resulting yields to be symmetric about $A = 120$. The result is shown as black squares connected by lines in Figs. 1 and 2.

The charge distribution for a given mass A was obtained using Wahl systematics [25]. For every heavy mass, the charge deviation ΔZ, the charge width parameter σ_Z, and the odd-even factors F_Z and F_N were calculated. For each heavy mass, the charge distribution was then determined using

$$P(Z|A) = \tfrac{1}{2} F(A) N(A) \left[\mathrm{erf}(V) - \mathrm{erf}(W)\right], \qquad (5)$$

where

$$V = \frac{Z - Z_p + 0.5}{\sigma_Z \sqrt{2}} \quad \text{and} \quad W = \frac{Z - Z_p - 0.5}{\sigma_Z \sqrt{2}}, \qquad (6)$$

and $\mathrm{erf}(x)$ represent the error function. The factor $N(A)$ is simply a normalization factor. The most probable charge is given by

$$Z_p = A_h \frac{Z_c}{A_c} + \Delta Z, \qquad (7)$$

where Z_c is the charge of the fissioning compound nucleus, that is, 94 in the case of plutonium isotopes. The odd-even factor $F(A)$ is calculated as

$$\begin{aligned} F(A) &= F_Z \times F_N && \text{for } Z \text{ even and } N \text{ even},\\ F(A) &= F_Z / F_N && \text{for } Z \text{ even and } N \text{ odd},\\ F(A) &= F_N / F_Z && \text{for } Z \text{ odd and } N \text{ even},\\ F(A) &= 1/(F_Z \times F_N) && \text{for } Z \text{ odd and } N \text{ odd}. \end{aligned}$$

The charge of the light fragment is simply given by $Z_l = Z_c - Z_h$.

The charge distribution obtained by integrating the final fragment distribution over the mass is shown in Fig. 3, and is in fair agreement with the results of Schmitt *et al.* [26] as

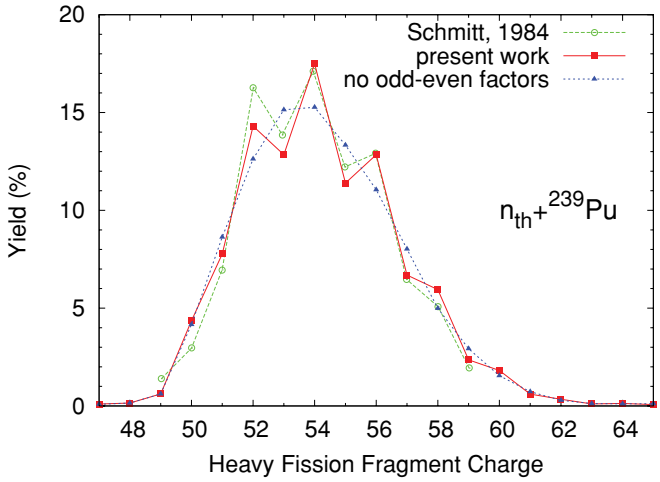

FIG. 3. (Color online) Fission fragment charge distribution vs heavy fragment charge for the thermal neutron-induced fission of ^{239}Pu. This curve was obtained by integrating the final fragment distribution $Y(A, Z)$ over masses A. Open circles show the experimental data of Schmitt *et al.* [26].

reported in Fig. 92 of Ref. [27]. Neglecting the factors $F(A)$ would smear the odd-even effects, as shown by the dotted line in Fig. 3.

Measurements of the average total kinetic energy per fragment mass $\langle TKE\rangle(A)$ and the width of the (assumed) Gaussian distribution $\sigma^2_{TKE}(A)$ were used to reconstruct the total kinetic energy distribution $Y(TKE)$. Figure 4 shows the measured data sets on $\langle TKE\rangle(A)$ from Wagemans *et al.* [21], Surin *et al.* [22], Asghar *et al.* [28], and Tsuchiya *et al.* [24], as well as the result of a least-square fit of the data. The data by Asghar *et al.* were taken directly from the published figure in Ref. [28] and correspond to the EXFOR entry number

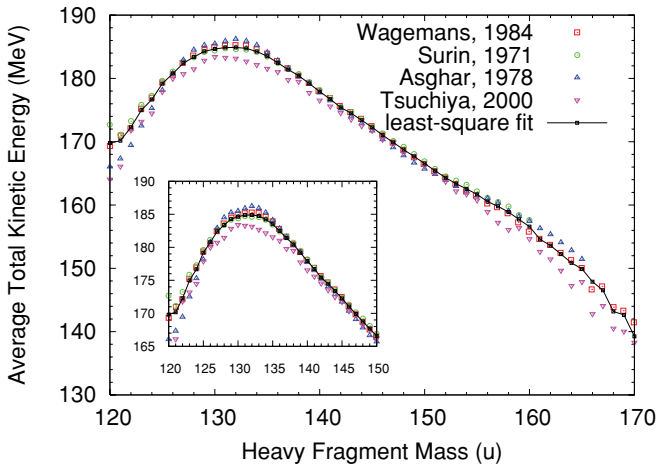

FIG. 4. (Color online) The average $\langle TKE\rangle$ is plotted as a function of the heavy fragment mass, as measured by Surin *et al.* [22], Asghar *et al.* [28], Wagemans *et al.* [21], and Tsuchiya *et al.* [24]. The inset shows a zoom on the region of TKE values between 165 and 190 MeV, where the fragment yields $Y(TKE)$ are maximum (see Fig. 7). The solid line and black squares show the result of a least-square fitting of the experimental data sets.

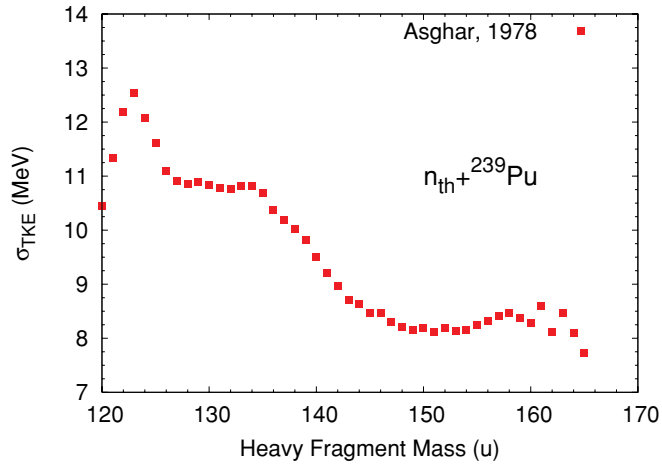

FIG. 5. (Color online) The width of the TKE distribution as a function of the fragment mass $\sigma_{TKE}(A)$ was measured by Asghar *et al.* [28] in the case of thermal neutron-induced fission of ^{239}Pu.

21544-010. As far as we understand, those data were not corrected for neutron emission. The measured average $\langle TKE\rangle$ is 176.0 MeV, while the value corrected for neutron emission is 177.9 MeV (see Table 1 in Ref. [28]), in close agreement with the data of Wagemans *et al.* We have rescaled the data of Asghar *et al.* to this higher $\langle TKE\rangle$ value before performing a least-square fit of all data sets.

The average width of the Gaussian $TKE(A)$ distribution has been reported by Asghar *et al.* [28] and is shown in Fig. 5.

The full fragment distribution was reconstructed following:

$$Y(A, Z, TKE) \simeq Y(A) \times P(Z|A) \times P(TKE|A)$$
$$\simeq Y(A) \times P(Z|A) \times \frac{1}{\sqrt{2\pi\sigma^2_{TKE}(A)}}$$
$$\times \exp\left\{-\frac{[TKE - \langle TKE\rangle(A)]^2}{2\sigma^2_{TKE}(A)}\right\}. \quad (8)$$

In this equation the mass distribution $Y(A)$ and $\langle TKE\rangle(A)$ were taken as the least-square fits obtained above, while

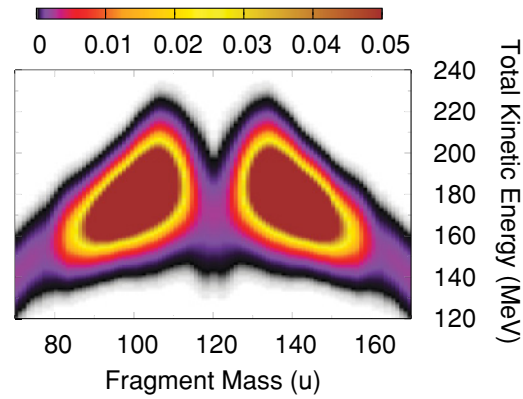

FIG. 6. (Color) Primary fission fragment yields as a function of mass and total kinetic energy. The units of the color scale are in percent.

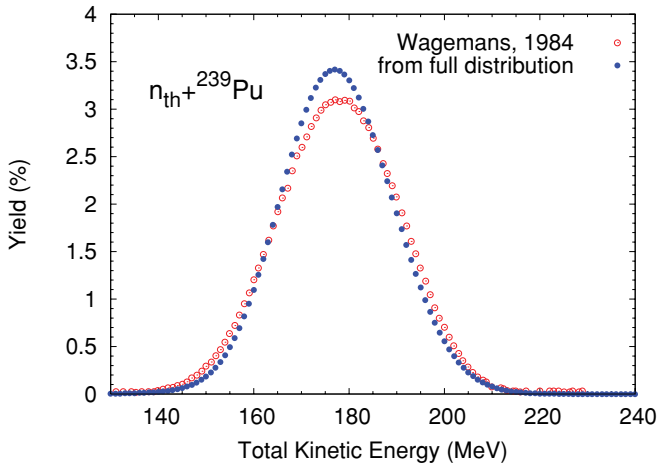

FIG. 7. (Color online) Primary fission fragment yields as a function of the total kinetic energy, projected from the full distribution $Y(A, Z, TKE)$ and measured by Wagemans [21]. The average TKE measured by Wagemans is 177.67 MeV, to be compared with 177.57 MeV obtained from the present work, and Asghar value of 177.9 MeV.

$\sigma^2_{TKE}(A)$ was taken from Asghar *et al.* [28]. The charge distribution $P(Z|A)$ was obtained from Eq. (5).

The final distribution $Y(A, TKE)$ is shown in Fig. 6 as a contour plot.

Mass and charge can be integrated out from the full fission fragment yield distribution $Y(A, Z, TKE)$ to obtain the distribution in total kinetic energy $Y(TKE)$. The result is shown in Fig. 7 and compared to the distribution given by Wagemans *et al.* [21]. The average energy obtained in this work is $\langle TKE \rangle = 177.57$ MeV, compared to the experimental value of 177.67 MeV in Ref. [21], and the value of Asghar *et al.* of 177.9 MeV, after neutron emission corrections are included. A correct description of the TKE distribution is particularly important to predict the average total prompt neutron multiplicity.

In the following, we are interested in the prompt fission neutron spectra for thermal as well as 0.5 MeV incident neutrons. Here we are making the approximation that the fission fragment yield distribution is the same at those two incident energies. Only the change of 0.5 MeV in excitation energy is taken into account.

IV. EXCITATION ENERGY SHARING AT SCISSION

The point when the two nascent fragments finally break apart is called the scission point. While the classical definition of the scission point is clear, its quantum-mechanical counterpart is ambiguous, at best. It is indeed difficult to mark a clear point in time and space where the two quantum systems in contact are finally noninteracting. Several definitions have been used and implemented in Hartree-Fock calculations for practical reasons [29,30], that is, to be able to answer questions on the mass and charge fragment yields, on the deformations of the fragments right at scission, and on the amount of excitation energy and angular momentum carried away by the fragments. All those questions are pertinent to the present discussion on prompt neutron emission.

In the original Madland-Nix model [3], the assumption was made that the two nascent fragments are in thermal equilibrium, and therefore that the total excitation energy is shared according to the level density in the light and heavy fragments, respectively. This assumption was carried forward to the fully accelerated fragments, that is, once they are fully separated and that they have relaxed into their respective ground-state deformations. Experiments tend to indicate that this assumption is not usually correct, as more neutrons are emitted from the light than from the heavy fragments.

In Ref. [16] the excitation energy sorting mechanism between two quantum systems in contact was investigated through the lens of fission dynamics, and the authors argue that the nascent fragments cannot share the same temperature at scission. This conclusion stems from one assumption and one observation: (i) it is assumed that the nascent fragments near scission are already in their equilibrated ground-state shape and (ii) a formula for the temperature of the fragments is inferred from observed level densities. The assumption of a constant-temperature formula is best suited to low excitation energies, and is part of the Gilbert-Cameron level density representation used in the present work. However, the distribution of excitation energies in the fission fragments extends to higher energies for which the Fermi-gas formula might be a better representation. It is also not clear that the fragments formed right at scission are close enough to their ground-state configuration that additional deformation energies can be neglected. So it is very possible that the fragments are indeed in thermal equilibrium near the scission point, but gain very different temperatures by the time they emit prompt neutrons and γ rays. However, some of our ongoing work on this problem suggests that indeed the sorting mechanism presented in Ref. [16] can explain a lot of the observed prompt neutron multiplicity data.

One way of predicting the behavior of the parameter R_T as a function of the fragment mass pair is to quantify the departure of the fragments from spherical shell closures. Such an approach was used by Dange *et al.* [31] to infer the deformation of the fission fragments in the case of thermal-neutron induced fission on ^{237}Np. The distance d between the center of mass of the two nascent fragments is first compared to the same distance if the two fragments are spherical and in contact: $r = r_l + r_h = r_0(A_l^{1/3} + A_h^{1/3})$. The ratio between the light and heavy fragments is then given by

$$d_{lh} = \frac{[(d-r)/r]_l}{[(d-r)/r]_h} = \frac{(N-N_l)+(P-Z_l)}{(N-N_h)+(P-Z_h)}, \qquad (9)$$

where N and P have the values 28, 50, or 82, depending on their proximity to the corresponding spherical closed shells. We have computed this equation using the fragment yields obtained above, and the result is shown in Fig. 8.

At symmetry of course the two fragments are similarly deformed, there is no way to distinguish one from the other. Moving away from symmetry, the light fragment becomes more deformed while its heavy counterpart gets closer to the doubly magic nucleus with $Z = 50$ and $N = 82$. The

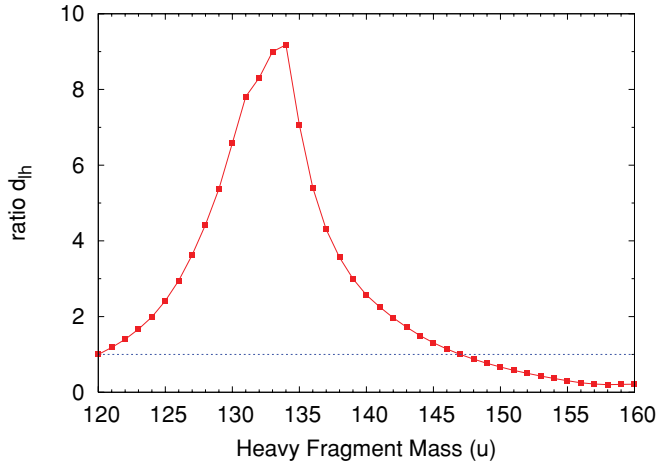

FIG. 8. (Color online) Distance of the fission fragments from spherical closed shells as computed by Eq. (9) and weighted for the charge and mass fission fragment yields $Y(A, Z)$.

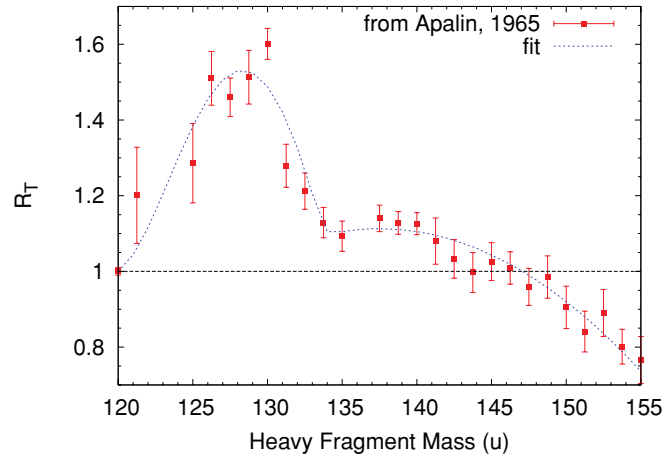

FIG. 9. (Color online) The temperature ratio parameter R_T is shown as a function of the heavy fragment mass. The data points were inferred by searching $R_T(A)$ that minimize discrepancies with $\overline{\nu}_l/\overline{\nu}_h$ using Apalin data [33]. The results were fitted with two functions for A in [120:135] and for [135:155].

parameter R_T is then greater than one. The difference between the two curves is maximum near $A = 132$, and we can expect R_T to reach its maximum in this mass region. Beyond $A \sim 135$, the heavy fragment departs from the spherical shell closure, and becomes even more deformed than the light fragment near $A \simeq 147$. At this point, R_T would decrease below 1.0.

A similar argument was used recently by Litaize and Serot [12] to justify their use of $R_T(A)$ parameters. However, this argument works only if the deformation of the fragments at scission are reasonably different from their ground-state configuration.

Both arguments, that either the fragments are already formed in their ground-state deformations with different temperatures or that the fragments gain deformation energies near scission, are plausible but none is conclusive. Also at this stage they remain qualitative only, and do not provide quantitative values for $R_T(A)$.

To perform the Monte Carlo simulations described above, we obtained $R_T(A)$ from a fit to experimental data on $\overline{\nu}_l/\overline{\nu}_h$ as a function of the heavy fragment mass. The average neutron multiplicity as a function of the fragment mass $\overline{\nu}(A)$ has been measured by several groups: Batenkov *et al.* [32], Tsuchiya *et al.* [24], Nishio *et al.* [20], and Apalin *et al.* [33]. However, the data of Batenkov *et al.* cannot be used as the measured mass range is too limited to compute the ratio of light vs heavy multiplicities. The data of Nishio *et al.*, on the other hand, have very large uncertainties. While they agree somewhat with Apalin data, those large uncertainties imply that they have no impact on our final fit. Finally, Tsuchiya data were obtained with a very large mass resolution and were not used in this fit.

The data of Apalin *et al.* were used for each mass pair, and the R_T parameter was inferred by minimizing the discrepancy between calculated and experimental values of $\overline{\nu}_l/\overline{\nu}_h$. The result is shown in Fig. 9. A polynomial fit was then used in two mass regions, [120:135] and [135:155]. In the mass region from 132 to 140, the R_T parameter is relatively flat near the value of 1.1. From symmetry to near 135, the data points can be fitted by an inverted parabola, which peaks near $A \sim 128$. For masses heavier than 140, the R_T parameter starts to decrease and falls below 1.0 near $A \sim 147$. The mass dependence of R_T as observed in this fit can be qualitatively explained by Eq. (9), as discussed above.

In the present work several calculations have been performed assuming different values for $R_T(A)$, from a constant equal to 1.0, 1.1, and 1.2, to using the full result $R_T(A)$ obtained from Fig. 9. In the next section we will discuss results obtained with either $R_T = 1.1$ and with $R_T(A)$ as estimated above. Note that results obtained with $R_T = 1.0$ led to a significant underprediction of the average PFNM from the light fragments $\overline{\nu}_l$, while $R_T = 1.2$ led to an overprediction of the same quantity.

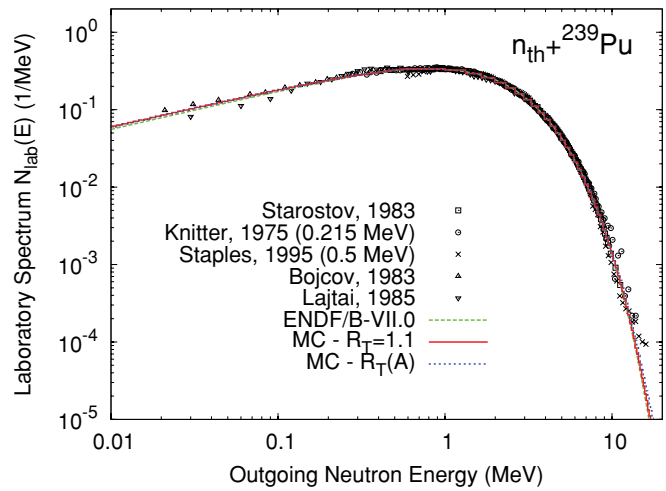

FIG. 10. (Color online) Average prompt fission neutron spectrum for nth + ^{239}Pu calculated with $R_T(A)$. Experimental data for incident neutron energies below 0.5 MeV are also plotted and were taken from Starostov *et al.* [36], Knitter and Budtz-Jørgensen [37], Staples *et al.* [38], Bojcov *et al.* [39], and Lajtai *et al.* [40].

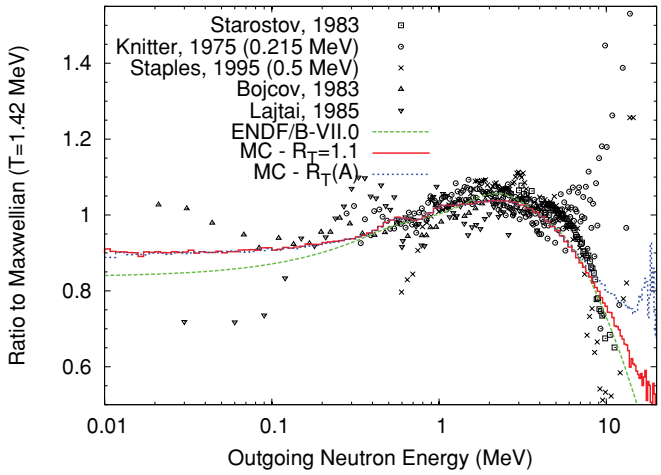

FIG. 11. (Color online) Same as Fig. 10 but shown as a ratio to a Maxwellian at temperature 1.42 MeV.

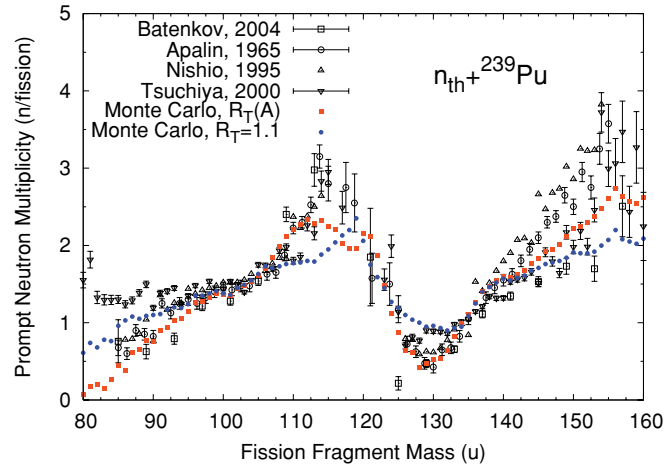

FIG. 12. (Color online) The average prompt fission neutron multiplicity (PFNM) is plotted as a function of the fragment mass. The Monte Carlo calculation is obtained using the mass-dependent $R_T(A)$ parameter (red squares) as well a constant value $R_T = 1.1$ (blue circles).

V. RESULTS AND DISCUSSION

The FFD code was written to implement the Monte Carlo evaporation model described above, and was used to obtain the following results.

While the Monte Carlo approach can predict results well beyond the average spectrum $\chi(E_{\text{out}})$ and neutron multiplicity $\overline{\nu}$, those two quantities are of major interest for the applied nuclear physics community are relatively well known and therefore can serve as a benchmark to the present calculations.

The average thermal prompt fission neutron spectrum calculated with $R_T(A)$ is shown in Figs. 10 and 11 in absolute units as well as in ratio to a Maxwellian at temperature $T = 1.42$ MeV. The calculated spectrum is in good agreement with experimental data and the ENDF/B-VII.0 evaluation [41] based on the Madland-Nix model in the energy range 0.3 –6.0 MeV. In the low energy trail of the spectrum, that is, below about 300 keV, the Monte Carlo result is 5%–10% higher than the ENDF/B-VII.0 result. The Monte Carlo spectrum also has a harder tail than the current evaluation, although the results there are very sensitive to the choice of the $R_T(A)$ parameters.

The low-energy tail of the spectrum is of great interest and has been intensely debated over the years [2,34,35]. Some authors have suggested that the Madland-Nix model, which considers neutrons emitted from *fully accelerated* fission fragments only, systematically underestimates the number of neutrons below about 500 keV. More recently, Maslov [34] has been able to get higher spectrum values in this energy range by introducing a new parametrization using 2 W spectra, with a new parameter similar to R_T, and an extra parameter α to describe emission of neutrons before the fragments reach full acceleration.

While those models do work in reproducing higher spectrum values in the low-energy tail of the spectrum, the values chosen for the parameters α and R_T are not explained or/and derived from physical considerations. In addition, since the models cannot calculate more than average values, they cannot be constrained by other, more exclusive, experimental data such as $\overline{\nu}(A)$.

The present Monte Carlo calculations also show higher values of PFNS below 300 keV, without the assumption of emission prior to full acceleration of the fragments. It is not to say that there is not such a mechanism occurring, but simply that this mechanism is not needed to explain the shape of the spectrum, and that, if it exists, its impact should be relatively small on the average spectrum itself. Note that this conclusion could change if more realistic neutron-γ competition is included in a full Hauser-Feshbach calculation.

As seen in Fig. 11, the high-energy tail of the spectrum is very sensitive to the R_T parameter. The spectrum gets harder with increasing excitation energy put into the light fragments at the expense of the heavy fragments. The reason is twofold: (i) the level density parameters tend to be smaller for light fragments, increasing the temperatures of the evaporation spectra and (ii) neutrons emitted from light fragments get a stronger kinematic boost than the ones emitted from heavy fragments. Hence increasing R_T leads to a harder spectrum.

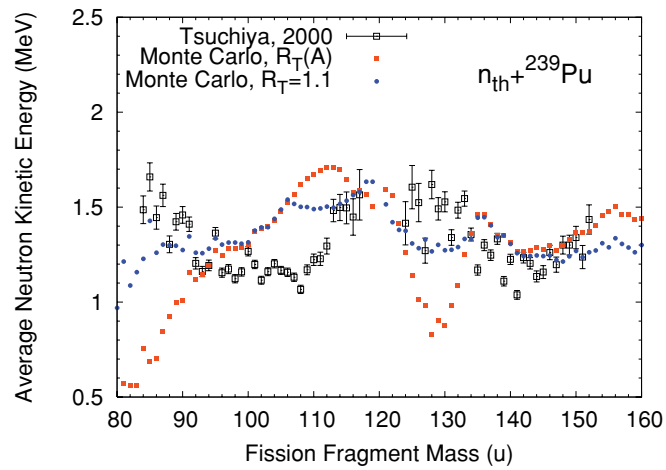

FIG. 13. (Color online) Average center-of-mass energy of the prompt fission neutrons as a function of the fragment mass.

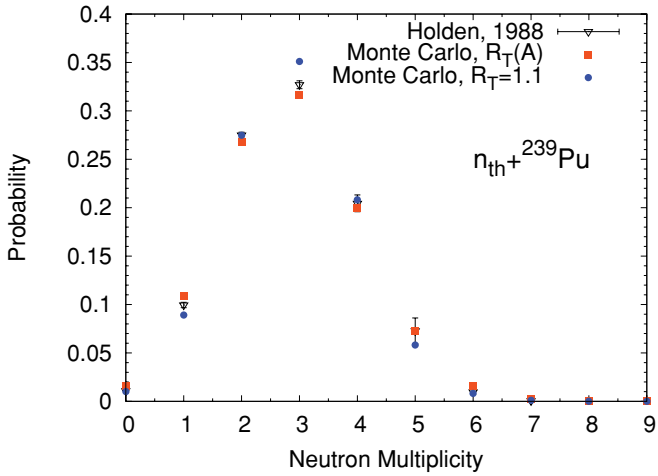

FIG. 14. (Color online) The calculated prompt fission neutron multiplicity distribution $P(\nu)$ is in very good agreement with the evaluation by Holden and Zucker [43], and is insensitive to the choice of the R_T parameter.

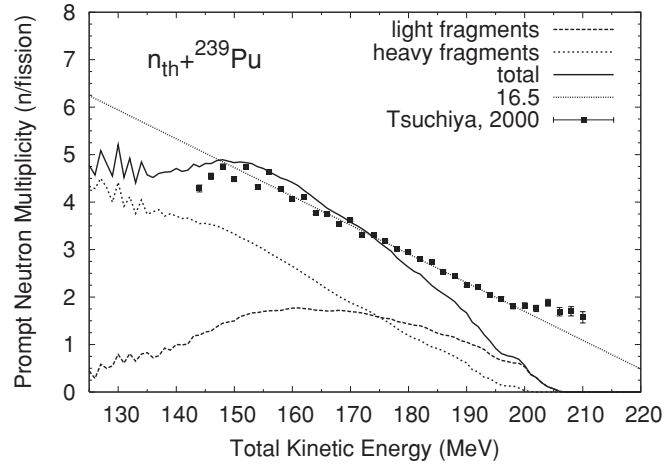

FIG. 15. The average prompt neutron multiplicity is plotted as a function of the total kinetic energy. The experimental data by Tsuchiya *et al.* [24] can be fitted by a straight line with slope -16.5 MeV^{-1}, while our numerical results indicate a slope of -10.5 MeV^{-1} instead.

The spectrum calculated with $R_T(A)$ is also much harder than the one obtained with a constant R_T value of 1.1. This increase is principally due to near-symmetric fission fragments for which $R_T(A)$ was estimated to reach a maximum (see Fig. 9). To recall, the mass dependence of R_T was obtained by fitting experimental data on $\overline{\nu}(A)$, and the result is shown in Fig. 12. While the agreement between calculation and experiment is indeed improved near $A \sim 130$, it is at the expenses of other quantities, such as the average center-of-mass neutron energy $\overline{\epsilon}_{\text{c.m.}}(A)$, shown in Fig. 13. In fact, we noted early in Ref. [7] that the average center-of-mass neutron energy could not be reproduced accurately in this mass region, as the initial excitation energies are too low to fully validate the Weisskopf evaporation formula. So, forcing the calculated values of the neutron multiplicity $\overline{\nu}(A)$ to agree with the experimental data for $A \sim 130$ may not be the wisest choice, and the spectra calculated with $R_T(A)$ shown in Fig. 11 should not be considered as the "best" result in the present work, but more as an indication of the uncertainties stemming from limitations of the present model.

The calculated average PFNM is $\overline{\nu}_{\text{calc}} = 2.871$, in very close agreement with the ENDF/B-VII.0 evaluated value of 2.8725 [41], and within one standard deviation from the value of 2.8771 ± 0.0047 evaluated by the IAEA Standards working group [42]. Also note that this calculated value depends only very slightly on the R_T parameter. The calculated average neutron multiplicity distribution $P(\nu)$ is shown in Fig. 14, compared to evaluated values from Holden and Zucker [43]. The calculated results are in good agreement with the evaluation. Note that in our original calculations for n (0.5 MeV) + ^{235}U and ^{252}Cf (sf), the calculated average prompt fission neutron multiplicities were systematically too high [7]. The results are slightly worse if one considers $R_T = 1.1$ only, but the average value $\overline{\nu}$ is nearly unchanged.

The average prompt neutron multiplicity $\overline{\nu}$ is shown in Fig. 15 as a function of the total kinetic energy. As TKE increases, the total excitation energy dissipated through the emission of prompt neutrons and γ rays decreases. Assuming that the average total energy dissipated by γ rays remains relatively constant as a function of TKE, we can conclude that less neutrons will be emitted when TKE increases. This is what is observed indeed. However, the present results do not agree with the experimental data points of Tsuchiya *et al.* [24] (also shown in Fig. 15) which predict a slope $-d\overline{\nu}/dTKE = 16.5^{-1}$ MeV^{-1}. Instead, our results are consistent with a slope of 10.5^{-1} MeV^{-1}.

Our calculated result is a direct consequence of the distribution of initial excitation energies available in the primary fragments, as shown in Fig. 16. For a total kinetic energy value of 200 MeV, the average initial excitation energy is about 10 MeV, to be shared among the light and heavy fragments. Considering the extreme case in which all the excitation energy available is fully transferred to one of the two fragments, only a maximum of one neutron would be emitted on average. More realistically, the average neutron multiplicity will be lower

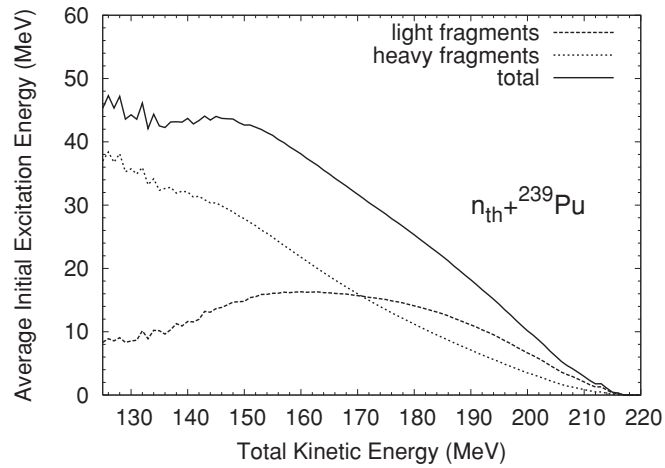

FIG. 16. (Color online) Average initial excitation energy in the primary fission fragments as a function of the total kinetic energy.

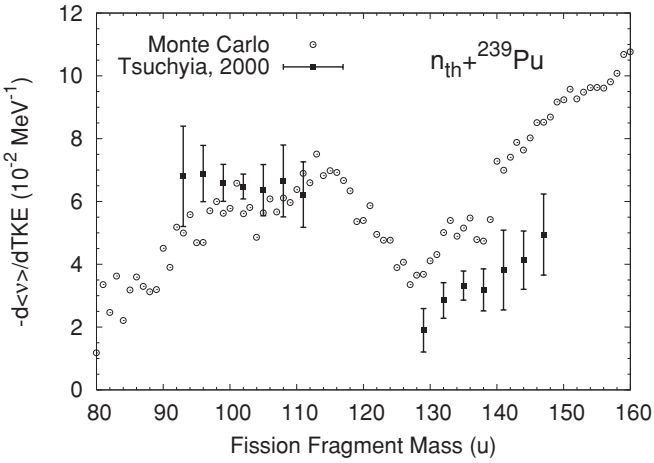

FIG. 17. The variation of $\overline{\nu}$ with TKE is plotted as a function of the fragment mass.

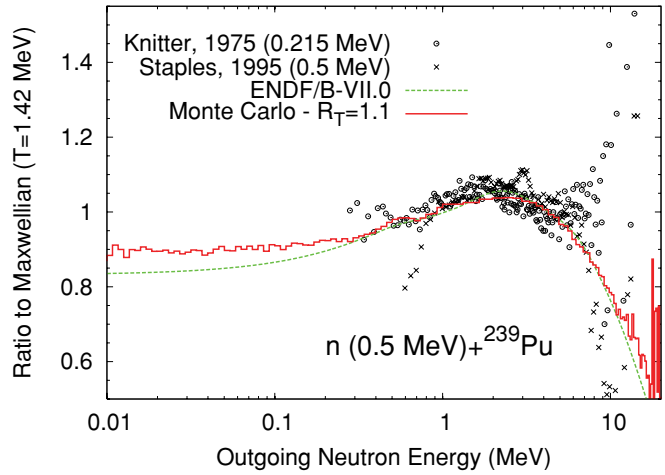

FIG. 18. (Color online) Ratio of average prompt fission neutron spectrum to Maxwellian, for 0.5 MeV incident neutrons on ^{239}Pu, and compared to experimental data for incident neutron energies near 0.5 MeV.

than 1, as shown by the calculated solid line in Fig. 15. On the contrary, data from Tsuchiya *et al.* indicate that close to two neutrons are emitted even for TKE values as high as 210 MeV.

Interestingly, the number of prompt neutrons emitted with decreasing TKE remains nearly flat below about 150 MeV. This result is simply due to the evolution of the Q value for the fission reaction in different mass regions spanned by different TKE values. It is most visible for the neutrons emitted from the light fragments (dashed line in Fig. 16) for which the average initial excitation energy decreases with decreasing total kinetic energy below about 160 MeV.

The variation of $-d\overline{\nu}/dTKE$ with the fragment mass A was calculated and is shown in Fig. 17. For each fragment mass, the variation of $\overline{\nu}$ with TKE was calculated and fitted with a linear function. This linear approximation was good in most, but not all cases, and may explain some fluctuations in the inferred slope coefficients shown in Fig. 17. Experimental results by Tsuchiya *et al.* [24] are also shown in Fig. 17. Our calculation agrees well with the experimental data for the light fragments, but overestimates the data points for the heavy fragments. The trend observed in the calculations is very similar to what was first observed in ^{252}Cf (sf) by Butdz-Jørgensen and Knitter [44]. The experimental points stop at $A_{\min} = 90$, below which our calculations predict a significant drop.

The saw-tooth behavior observed on $-d\overline{\nu}/dTKE(A)$ was explained qualitatively by Brosa *et al.* in the framework of the random-neck-rupture model [45] as due to the presence of rigid pre-scission fragments at spherical shell closures (near 28, 50, and 82 proton and neutron numbers).

While the previous results were obtained for thermal incident neutrons, evaluating the prompt fission neutron spectrum at higher incident energies is also of great importance. In particular the PFNS for fast incident neutrons in the few hundred kilo-electron-volt region is of interest for various applications, including fast Generation-IV nuclear reactors. We have calculated the PFNS for 0.5 MeV incident neutrons by assuming the same fission fragment distribution $Y(A, Z, TKE)$ and adding 0.5 MeV of total excitation energy.

The spectrum calculated for 0.5 MeV incident neutrons and with $R_T = 1.1$ is shown in Fig. 18 in very good agreement with the ENDF/B-VII.0 evaluated spectrum over the well-measured energy range, but deviating from it for the lowest (below 300 keV) and highest (above 10 MeV) outgoing energies.

The average neutron multiplicity calculated for 0.5 MeV incident neutrons is $\overline{\nu}_c = 2.932$, in very good agreement with the evaluated value of 2.939 in ENDF/B-VII.0.

Recent experimental efforts at the LANSCE, Los Alamos Neutron Science Center, have led to the measurement of PFNS for n+^{239}Pu for incident neutron energies from 1 up to 200 MeV [46]. A comparison of our calculated spectrum at 0.5 MeV incident neutron energy with LANSCE data for incident energies between 1 and 2 MeV is shown in Fig. 19. Within the relatively large reported experimental uncertainties, the data points agree very well with both the ENDF/B-VII.0 evaluation

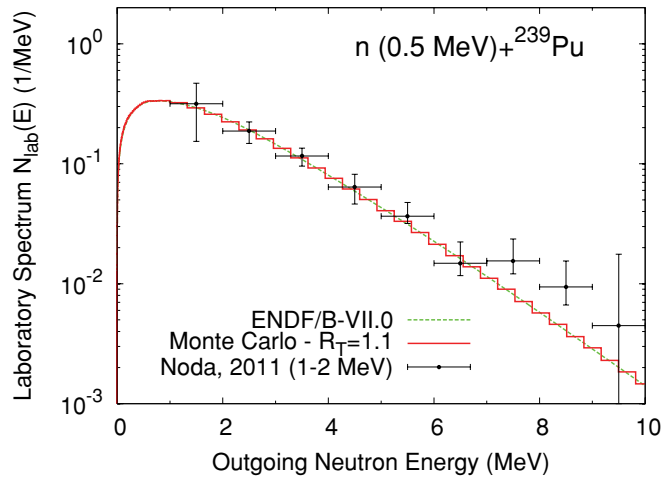

FIG. 19. (Color online) The average PFNS calculated at 0.5 MeV is compared to recent experimental data by Noda *et al.* [46] for incident neutron energies from 1 to 2 MeV, as well as with the ENDF/B-VII.0 evaluated PFNS at 0.5 MeV.

and our Monte Carlo result, except for the highest outgoing energies above 7 MeV. Unfortunately, the large experimental uncertainties cannot distinguish between the two calculations, pointing toward the need for more precise experimental data as well as extending the measurement to the lowest energies below 1 MeV.

VI. CONCLUSION

The Monte Carlo calculations presented in this work follow the decay of primary fission fragments by evaporating prompt fission neutrons. γ rays are not considered in this work, and are simply assumed to be emitted after the sequence of neutron emissions is complete. In particular, we have studied the decay of excited fission fragments following the neutron-induced fission of ^{239}Pu for incident neutrons at thermal and 0.5 MeV energies.

For both incident energies, the Monte Carlo calculated spectra agree reasonably well with the Madland-Nix model calculations in the outgoing energy range of about 0.3 to 6 MeV. Below 300 keV the Monte Carlo PFNS is 5%–10% higher than the MN spectrum. It is also harder in the high-energy tail of the spectrum, above about 6 MeV. Some assumptions had to be made on the sharing of the total excitation energy between the two fragments at scission. Fair agreement with experimental data on $\overline{\nu}_l/\overline{\nu}_h$ was obtained for a temperature ratio parameter $R_T \simeq 1.1$. An even better agreement can be obtained by fitting $R_T(A)$ to the ratio $\overline{\nu}_l/\overline{\nu}_h$ for each fragment mass pair (A_l, A_h). However, the average outgoing neutron energy as a function of mass $\overline{\epsilon}_{\text{c.m.}}(A)$ is calculated poorly in this case, and the calculated average spectrum may be too hard. The discrepancy between calculation and experimental data on $\overline{\epsilon}_{\text{c.m.}}(A)$ is particularly bad for fragments near a spherical closed shell, for which the available initial excitation energy is low. In this case, our model based on the Weisskopf evaporation assumption is not expected to apply anymore.

An equitemperature assumption whereby the light and heavy fragments have the same temperature $T_l = T_h$ leads to an underprediction of $\overline{\nu}$ for the light fragments and a corresponding overprediction for the heavy fragments. This conclusion agrees well with previous studies [15,16].

The Monte Carlo simulations predict $P(\nu)$ in very good agreement with the evaluation by Holden and Zucker [43], while the average calculated $\overline{\nu}_c = 2.871$ is very close to the ENDF/B-VII.0 evaluated value of 2.8725 and in reasonable agreement with the Standards evaluation value of 2.8836. This result is nearly independent on the assumption made for the temperature ratio parameter R_T.

The calculations presented here represent an important step toward a much improved understanding of prompt fission neutrons. By calculating prompt fission neutron data beyond the ubiquitous average spectrum and multiplicity, this Monte Carlo approach is well suited for detailed analyses of advanced experimental measurements in which correlations and exclusive data are obtained. It provides an important tool for better understanding the link between pre- and postscission physics, and in particular constrain theoretical models of fission that aim at predicting fission fragment yields as a function of mass, charge, and kinetic energy. Additional constraints on this Monte Carlo approach and the remaining free parameters are expected from simultaneous studies of other isotopes such as ^{235}U and ^{252}Cf (sf) for which relatively good experimental data exist.

However, significant experimental efforts should be devoted to the study of the low (below 500 keV) and high (above 6 MeV) energy tails of the PFNS, as it would place significant constraints on the Monte Carlo model parameters. As we believe that studying the average prompt fission neutron spectrum is not enough to unambiguously answer the question of the existence of scission neutrons, more emphasis should be placed on measurements of neutron-neutron correlations (angle, energy) as well on the angular distributions of the emitted neutrons with respect to the direction of the fission fragments.

The present calculations can be further extended by properly considering the neutron-γ competition in a full Hauser-Feshbach framework, as has been done already for nonfission studies [13]. In this regard, experimental efforts to measure prompt fission γ (spectrum, multiplicity, etc) are of great interest.

[1] P. Talou, T. Kawano, D. G. Madland, A. C. Kahler, D. K. Parsons, M. C. White, R. C. Little, and M. B. Chadwick, Nucl. Sci. Eng. **166**, 254 (2010).
[2] N. V. Kornilov, A. B. Kagalenko, S. V. Poupko, P. A. Androsenko, and F.-J. Hambsch, Nucl. Phys. A **686**, 187 (2001).
[3] D. G. Madland and J. R. Nix, Nucl. Sci. Eng. **81**, 213 (1982).
[4] G. Vladuca and A. Tudora, Ann. Nucl. Energy **28**, 419 (2001).
[5] A. Tudora, Ann. Nucl. Energy **36**, 72 (2009).
[6] T. Ohsawa, T. Horiguchi, and M. Mitsuhashi, Nucl. Phys. A **665**, 3 (2000).
[7] S. Lemaire, P. Talou, T. Kawano, M. B. Chadwick, and D. G. Madland, Phys. Rev. C **72**, 024601 (2005).
[8] S. Lemaire, P. Talou, T. Kawano, M. B. Chadwick, and D. G. Madland, Phys. Rev. C **73**, 014602 (2006).
[9] J. C. Browne and F. S. Dietrich, Phys. Rev. C **10**, 2545 (1974).
[10] J. Randrup and R. Vogt, Phys. Rev. C **80**, 024601 (2009).
[11] R. Vogt, J. Randrup, J. Pruet, and W. Younes, Phys. Rev. C **80**, 044611 (2009).
[12] O. Litaize and O. Serot, Phys. Rev. C **82**, 054616 (2010).
[13] T. Kawano, P. Talou, M. B. Chadwick, and T. Watanabe, J. Nucl. Sci. Technol. **47**, 462 (2010).
[14] F. Gönnenwein, in *The Nuclear Fission Process*, edited by C. Wagemans (CRC Press, Boca Raton, FL, 1991), p. 396.
[15] P. Talou, T. Kawano, O. Bouland, J. E. Lynn, P. Möller, and M. B. Chadwick, Proceedings of the International Conference on Nuclear Data for Science & Technology ND2010, April 26–30, 2010, Jeju Island, Korea.
[16] K.-H. Schmidt and B. Jurado, Phys. Rev. Lett. **104**, 212501 (2010).
[17] A. Gilbert and A. G. W. Cameron, Can. J. Phys. **43**, 1446 (1965).
[18] A. V. Ignatyuk, K. K. Istekov, and G. N. Smirenkin, Sov. J. Nucl. Phys. **29**, 450 (1979).

[19] V. Weisskopf, Phys. Rev. **52**, 295 (1937).
[20] K. Nishio, Y. Nakagome, I. Kanno, and I. Kimura, J. Nucl. Sci. Technol. **32**, 404 (1995).
[21] C. Wagemans, E. Allaert, A. Deruytter, R. Barthélémy, and P. Schillebeeckx, Phys. Rev. C **30**, 218 (1984).
[22] V. M. Surin, A. I. Sergachev, N. I. Rezchikov, and B. D. Kuzminov, Yad. Fiz. **14**, 935 (1971).
[23] N. I. Akimov, V. G. Vorobeva, V. N. Kabenin, N. P. Kolosov, B. D. Kuzminov, A. I. Sergachev, L. D. Smirenkina, and M. Z. Tarasko, Yad. Fiz. **13**, 484 (1971).
[24] C. Tsuchiya, Y. Nakagome, H. Yamana, H. Moriyama, K. Nishio, I. Kanno, K. Shin, and I. Kimura, J. Nucl. Sci. Technol. **37**, 941 (2000).
[25] A. C. Wahl, LANL Report LA-13928 (2002).
[26] C. Schmitt *et al.*, Nucl. Phys. A **430**, 21 (1984).
[27] C. Wagemans, Editor, *The Nuclear Fission Process* (CRC Press, Boca Raton, FL, 1991).
[28] M. Asghar, F. Caitucoli, P. Perrin, and C. Wagemans, Nucl. Phys. A **311**, 205 (1978).
[29] W. Younes and D. Gogny, Phys. Rev. C **80**, 054313 (2009).
[30] N. Dubray, H. Goutte, and J.-P. Delaroche, Phys. Rev. C **77**, 014310 (2008).
[31] S. P. Dange, A. Ramaswami, S. B. Manohar, S. Prakash, and M. V. Ramaniah, Phys. Rev. C **11**, 1251 (1975).
[32] O. A. Batenkov, G. A. Boykov, F.-J. Hambsch, J. H. Hamilton, V. A. Jakovlev, V. A. Kalinin, A. B. Laptev, V. E. Sokolov, and A. S. Vorobyev, AIP Conf. Proc. **769**, 1003 (2004).
[33] V. F. Apalin, Yu.N. Gritsyuk, I. E. Kutikov, V. I. Lebedev, and L. A. Mikaelian, Nucl. Phys. **71**, 553 (1965).
[34] V. M. Maslov, N. A. Tetereva, V. G. Pronyaev, A. B. Kagalenko, T. Granier, and B. Morillon, Proceedings of the Third International Conference on Current Problems in Nuclear Physics and Atomic Energy, Kyiv, Ukraine, June 7–12, 2010.
[35] N. Kornilov, F.-J. Hambsch, and A. S. Vorobyev, Nucl. Phys. A **789**, 55 (2007).
[36] V. N. Nefedov, B. I. Starostov, and A. A. Boytsov, Proceedings of the 6th All Union Conference on Neutron Physics, Kiev, 2–6 October 1983, p. 285, EXFOR entry 40871-006 (1983).
[37] H-H. Knitter and C. Budtz-Jørgensen, Nucl. Sci. Eng. **99**, 1 (1988).
[38] P. Staples, J. J. Egan, G. H. R. Kegel, A. Mittler, and M. L. Woodring, Nucl. Phys. A **591**, 41 (1995).
[39] A. A. Bojcov, A. F. Semenov, and B. I. Starostov, Proceedings of the 6th All Union Conference on Neutron Physics, Kiev, 2–6 October 1983, p. 294, EXFOR entry 40873-006 (1983).
[40] A. Lajtai, J. Kecskeméti, J. Sáfár, P. P. Dyachenko, and V. M. Piksaikin, *Proceedings of the International Conference on Nuclear Data for Basic and Applied Science*, edited by P. G. Young, R. E. Brown, G. F. Auchampaugh, P. W. Lisowski, and L. Stewart (Gordon and Breach, New York, 1985), Vol. 1, p. 613.
[41] M. B. Chadwick *et al.*, Nucl. Data Sheets **107**, 2931 (2006).
[42] International Evaluation of Neutron Cross-Section Standards, IAEA Technical Report (2007); A. D. Carlson *et al.*, Nucl. Data Sheets **110**, 3215 (2009).
[43] N. E. Holden and M. S. Zucker, Nucl. Sci. Eng. **98**, 174 (1988).
[44] C. Budtz-Jørgensen and H.-H. Knitter, Nucl. Phys. A **490**, 307 (1988).
[45] U. Brosa, S. Grossmann, and A. Müller, Phys. Rep. **197**(4), 167 (1990).
[46] S. Noda *et al.*, Phys. Rev. C **83**, 034604 (2011).